ELSEVIER

Chemical Engineering Journal 118 (2006) 119–125

Chemical Engineering Journal

www.elsevier.com/locate/cej

Complete oxidation of formaldehyde over Ag/MnO_x–CeO_2 catalysts

Xingfu Tang, Junli Chen, Yonggang Li, Yong Li, Yide Xu, Wenjie Shen *

State Key Laboratory of Catalysis, Dalian Institute of Chemical Physics, Chinese Academy of Sciences, Dalian 116023, China

Received 22 September 2005; received in revised form 7 February 2006; accepted 9 February 2006

Abstract

Complete oxidization of formaldehyde into harmless water and carbon dioxide was obtained over Ag/MnO_x–CeO_2 catalysts at a temperature as low as 373 K. Structural analysis by X-ray powder diffraction (XRD), X-ray photoelectron spectra (XPS) and temperature-programmed reduction (TPR) measurements revealed that the formation of MnO_x–CeO_2 solid solution and the subsequent addition of silver species resulted in significant improvement in the effective activation of oxygen molecules in the reaction stream. Accordingly, a consecutive oxygen transfer mechanism starting from the oxygen reservoir of CeO_2 to active Ag_2O sites through MnO_x was proposed. The oxygen species released from the decomposition of Ag_2O participated in the oxidation of formaldehyde, and the reoxidation of Ag to Ag_2O was achieved through the oxygen species from MnO_2. Simultaneously, the transformation of the produced Mn_2O_3 to MnO_2 was realized by the oxygen species from the oxygen reservoir of CeO_2, and the Ce_2O_3 thus formed can be reoxidized into CeO_2 by the oxygen in the feed stream. Such a consecutive oxygen pathway was suggested to play an important role in the complete oxidation of formaldehyde.

Keywords: Ag/MnO_x–CeO_2; Formaldehyde; Complete oxidation; Molecular oxygen activation

1. Introduction

Formaldehyde is becoming a major indoor pollutant in air-tight buildings, which is mainly emitted from the widely used constructive and decorative materials. It is recognized that long-term exposure to indoor air even containing a few ppm of formaldehyde may cause adverse effects on human health. Thus, great efforts have been made to reduce the indoor emission of HCHO for satisfying the stringent environmental regulations. Physical absorption with porous materials and chemical reaction with impregnated potassium permanganate and/or organic amines on the adsorption materials were found to be effective for eliminating formaldehyde emission in a certain short period [1,2]. However, the overall efficiency of these adsorbent materials was not so promising because of the limited removal capacities. Heterogeneous catalytic oxidation of HCHO into harmless CO_2 and H_2O has attracted wide attention in recent years for indoor air purification. Supported noble metals were proved to be promising catalysts for this application at lower temperatures. For instance, complete oxidation of HCHO was achieved over supported Ru, Pd and Pt catalysts in the temperature range of 363–473 K [3–5]. More recently, complete conversion of HCHO was obtained over a Pt/TiO_2 catalyst even at room temperature [6].

It also should be noted that mixed transition metal oxides, such as MnO_x and CeO_2, showed catalytic activities as high as or slightly higher than those of the supported noble metals for complete oxidation of formaldehyde [7,8]. A favorable synergetic effect between the metal oxides was attributed to the improvement in the oxidation activity of HCHO. Indeed, MnO_x–CeO_2 mixed oxides were developed as environmentally friendly catalysts for the abatement of contaminants both in the liquid phase and the gaseous phase [9–12]. It has been demonstrated that the MnO_x–CeO_2 mixed oxides had much higher catalytic activity than those of pure MnO_x and CeO_2 owing to the formation of solid solutions between the manganese and cerium oxides [12]. Our previous work has also confirmed that the MnO_x–CeO_2 mixed oxides could exhibit high catalytic activity for the complete oxidation of formaldehyde at 373 K [13]. Meanwhile, silver supported on these metal oxides has also been proved to be efficient in gas-phase catalytic combustion of volatile organic compounds. For example, the Ag/CeO_2 catalyst was found to be active for oxidative decomposition of formaldehyde above 423 K [7]. Larachi and coworkers found

* Corresponding author. Tel.: +86 411 84379850; fax: +86 411 84694447.
E-mail address: shen98@dicp.ac.cn (W. Shen).

1385-8947/$ – see front matter © 2006 Elsevier B.V. All rights reserved.
doi:10.1016/j.cej.2006.02.002

that Ag/MnO_x–CeO_2 exhibited the same catalytic performance as Pd/MnO_x–CeO_2 in wet oxidation of phenol [14].

With this background, the aim of the present work was to study the effect of silver addition to the MnO_x–CeO_2 mixed oxide on the complete oxidation of formaldehyde. Structure analysis of the catalysts were performed with XRD, H_2-TPR and XPS, and subsequently correlated with the catalytic behavior. It was found that improvement of the catalytic activity by silver addition could be attributed to the increase in the oxygen molecule activation capacity on the surface of the catalysts and to the acceleration of oxygen mobility among silver, manganese and cerium. Accordingly, a consecutive oxygen transferring steps from the oxygen reservoir CeO_2 to the active Ag_2O centers through MnO_x was proposed.

2. Experimental

2.1. Catalyst preparation

MnO_x–CeO_2 mixed oxide (Mn/(Mn + Ce) = 0.5, molar ratio) was prepared by the coprecipitation method. Typically, a 2 M NaOH solution was added slowly to a solution containing $Mn(NO_3)_2{\cdot}6H_2O$ and $Ce(NO_3)_3{\cdot}6H_2O$ at 323 K until the pH value of the mixture reached 10.5 under stirring. The precipitate was further aged at 323 K for 2 h in the mother liquid. After filtration and washing with distilled water, the as-prepared solid was dried at 383 K for 12 h and calcinated at 773 K for 6 h in air. Pure MnO_x and CeO_2 were prepared by precipitating $Mn(NO_3)_2{\cdot}6H_2O$ and $Ce(NO_3)_3{\cdot}6H_2O$, respectively, with a 2 M NaOH aqueous solution at 323 K according to the same procedure mentioned above. The obtained precipitates were also dried at 383 K for 12 h and calcined at 773 K for 6 h in air.

Ag/MnO_x–CeO_2 catalyst with silver loading of 3 wt.% was prepared by a deposition precipitation method. The MnO_x–CeO_2 powder were initially dispersed in an aqueous solution of $AgNO_3$, to which 0.25 M NaOH solution was then added slowly at 323 K until the pH value of the mixed solution reached 10.0. The precipitate was then further aged at 323 K for 3 h in the mother liquid under stirring. After filtration and washing with water, the obtained solid was dried at 383 K for 12 h and calcinated at 773 K for 6 h in air. For composition, the Ag/MnO_x and Ag/CeO_2 catalysts were prepared by the same procedure, in which the silver loading was also designed to be 3 wt.% for both cases with respect to the corresponding supports.

2.2. Catalyst characterization

N_2 adsorption isotherms of the samples were performed at 77 K using a Micromeritics ASAP 2000 analyzer. Specific surface areas were determined by using the linear portion of the BET plot and the average pore sizes were calculated by using the Barrett–Jovner–Halenda (BJH) formula from the desorption branch of the N_2 adsorption isotherm. Prior to the measurement, the samples were degassed in vacuum at 573 K for 2 h.

Elemental analysis was performed by inductively coupled plasma-atomic emission spectroscopy (ICP-AES) on a Plasam-Spec-I spectrometer.

X-ray powder diffraction (XRD) patterns were recorded on a D/Max-2500/PC powder diffractometer (Rigaku, Japan) using nickel-filtered Cu Kα radiation operating at 40 kV and 250 mA. The average crystallite sizes were calculated from the half-width of the ceria (1 1 1) peak or the Mn_2O_3 (Bixbyite-C) (2 2 2) peak according to the Scherrer's equation, where the Scherrer constant (particle shape factor) was taken to be 0.89. The lattice parameters were calculated according to the Cohen procedure [15].

Temperature-programmed reduction (TPR) measurements were carried out on a CHEMBET 3000 adsorption instrument (Quantachrome, USA) equipped with a TCD detector. Thirty to 50 mg samples were loaded and pretreated with He at 573 K for 1 h to remove the adsorbed carbonates and hydrates. After cooling down to 373 K and introducing the reduction gas of 5% H_2/Ar at a flow rate of 50 mL/min, the temperature was then programmed to rise at a ramp of 10 K/min up to 973 K.

X-ray photoelectron spectra (XPS) were recorded at room temperature on a KROTAS AMICAS spectrometer (Shimadzu, Japan) with a magnesium anode for Kα ($h\nu$ = 1253.6 eV) radiation. Charging effects were corrected by adjusting the binding energy of the C 1s peak to 284.6 eV. The spectra were deconvoluted using the XPSPEAK program by curve fitting, with a Gaussian/Lorentaian ratio of 90/10 after smoothing and subtraction of the Shirley-type background.

2.3. Activity measurement

Formaldehyde oxidation was performed in a fixed-bed reactor under atmospheric pressure within a temperature range of 313–503 K. Two hundred milligrams of catalyst (40–60 mesh) was sandwiched by quartz wool layers in a quartz tube reactor (i.d. = 6 mm). Gaseous HCHO was generated by flowing He over paraformaldehyde (96%, ACROS ORGANICS) in an incubator kept at 323 K. The HCHO/He stream was then mixed with the main gas stream of O_2/He, leading to a typical feed gas composition of 580 ppm HCHO and 18.0 vol.% oxygen, and balanced by helium. The total flow rate was 100 mL/min, corresponding to a gas hourly space velocity (GHSV) of 30,000 mL/(g_{cat} h). The effluents from the reactor were analyzed by on-line gas chromatograph equipped with TCD and FID detectors. To determine the exact concentration of produced carbon dioxide, a nickel catalyst converter was placed before the FID detector and used for converting CO_2 quantitatively into methane in the presence of hydrogen. In typical runs, the reaction data were obtained after HCHO oxidation was performed for 3 h in order to achieve the steady state. No other carbon containing compounds except CO_2 in the products were detected for all the tested catalysts. Thus, HCHO conversion was calculated as follows:

$$\text{HCHO conversion}\,(\%) = \frac{[CO_2]_{out}\,(\text{vol.}\%)}{[HCHO]_{in}\,(\text{vol.}\%)} \times 100,$$

where $[CO_2]_{out}$ is the CO_2 concentration in the products (vol.%) and $[HCHO]_{in}$ is HCHO concentration of the feed gas (vol.%).

Table 1
Textural characteristics of the samples

Sample	Ag (wt.%)	S_{BET} (m^2/g)	V_{pore} (cm^3/g)	D_{pore} (nm)	Particle size (nm)	Lattice parameter (nm)
MnO_x	–	9.6	0.067	30.3	34.1	0.9417
Ag/MnO_x	3.1	8.9	0.063	32.7	34.2[a]	0.9417[a]
CeO_2	–	49.0	0.160	9.7	16.6	0.5416
Ag/CeO_2	2.9	42.6	0.140	12.1	16.6	0.5416
MnO_x–CeO_2	–	141.1	0.312	6.9	4.1	0.5358
Ag/MnO_x–CeO_2	3.0	122.4	0.294	7.6	4.1	0.5358

[a] Particle size and lattice parameter refer to those of Mn_2O_3 (Bixbyite-C) in the Ag/MnO_x.

3. Results and discussion

3.1. Structure and redox properties of catalysts

Table 1 summarizes the physical and chemical properties of the oxides as well as the corresponding Ag catalysts. Obviously, the surface areas and the pore volumes of the manganese–cerium mixed oxide are much larger than those of the pure manganese and cerium oxides, indicating that the coprecipitation of manganese and cerium hydroxides and the possible interaction during calcination effectively inhibited the crystal growth of the MnO_x–CeO_2 mixed oxide. As a result, the pore size of the MnO_x–CeO_2 mixed oxide becomes smaller than the pure MnO_x and CeO_2. The loading of 3 wt.% silver only caused slight changes in the textural features of the oxides, since the surface areas of the oxides only marginally decreased by the addition of silver.

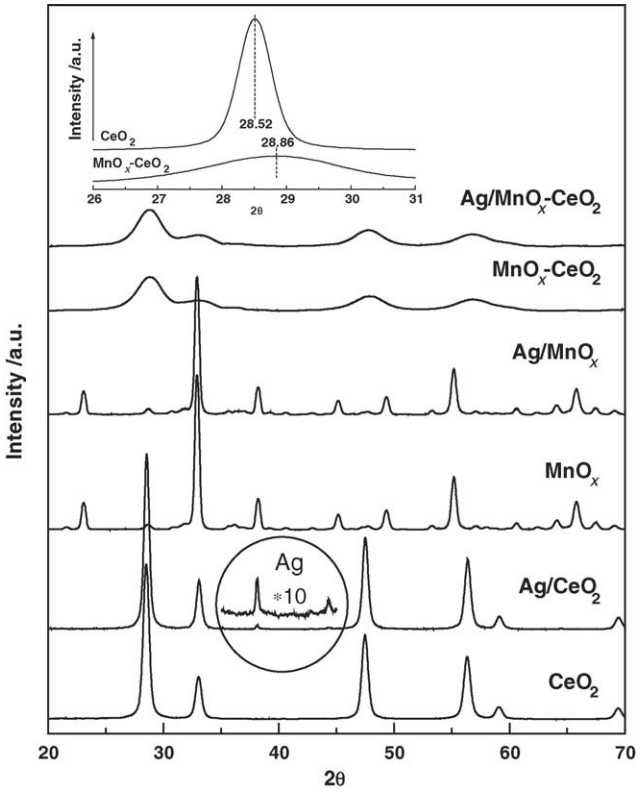

Fig. 1. XRD patterns of the oxides and the Ag catalysts.

Fig. 1 shows the XRD patterns of the samples, and the calculated average particle sizes and lattice parameters are listed in Table 1. For pure MnO_x, the intensive and sharp diffractions at $2\theta = 23.1°$, 32.9°, 38.2° and 55.2° could be primarily attributed to Mn_2O_3 (Bixbyite-C, PDF# 41-1442). The diffraction peaks at $2\theta = 28.5°$, 33.0°, 47.4° and 56.4° in the XRD profile of the pure cerium oxide clearly demonstrated the presence of cubic fluorite structure of CeO_2 (PDF# 43-1002). However, the XRD pattern of the MnO_x–CeO_2 mixed oxide did not show any diffraction of manganese oxides, and only broad reflections due to CeO_2 were observed. This is in good consistent with recent observations that the phase composition of MnO_x–CeO_2 mixed oxides strongly depended on the molar ratios of manganese and cerium oxides [16]. The diffraction patterns of MnO_x–CeO_2 mixed oxides at $Mn/(Mn + Ce) \geq 0.75$ showed crystallization of Mn_2O_3, whereas those at $Mn/(Mn + Ce) \leq 0.5$ consisted of only broad peaks attributed to CeO_2 due to the formation of solid solution between Mn_2O_3 and CeO_2. For the present MnO_x–CeO_2 oxide system, the $Mn/(Mn + Ce)$ ratio was designed to be 0.5, and it was highly possible to form solid solution during the precipitation and calcination processes. This can be further evidenced by the fact that the diffraction peaks of CeO_2 in the mixed oxide are slightly shifted to higher values of the Bragg angles, compared with the pure ceria. Since the ionic radius of Mn^{3+} (0.066 nm) is smaller than that of the Ce^{4+} (0.094 nm), the incorporation of Mn^{3+} into the ceria lattice to form MnO_x–CeO_2 solid solution would result in remarkable decrease in the lattice parameter of ceria (0.5358 nm) in the MnO_x–CeO_2 mixed oxide. After sliver was loaded, the average particle sizes and lattice parameters of the oxides remained almost unchanged, indicating that the silver species were highly dispersed on the surface of the supports. For the Ag/MnO_x and Ag/MnO_x–CeO_2 catalysts, the intensive and sharp diffraction peaks could still be attributed to their corresponding supports, and no diffraction peaks due to the Ag species could be observed. While, only discernable diffraction peaks at $2\theta = 38.1°$, 44.3° and 64.4°, which could be assigned to metal silver (PDF# 65-2871), appeared for the Ag/CeO_2 catalyst. This is similar to the observations of Imamura et al. [17].

Fig. 2 shows the H_2-TPR profiles of the oxides and the corresponding Ag catalysts. Similar to previous findings [18,19], pure CeO_2 showed weak and broad reduction peak with a maximum at about 846 K, representing the reduction of surface oxygen of ceria. The H_2-TPR profile of pure MnO_x showed two strong reduction peaks at 672 and 784 K, respectively, with an area ratio of the lower to the higher temperature hydrogen consumption

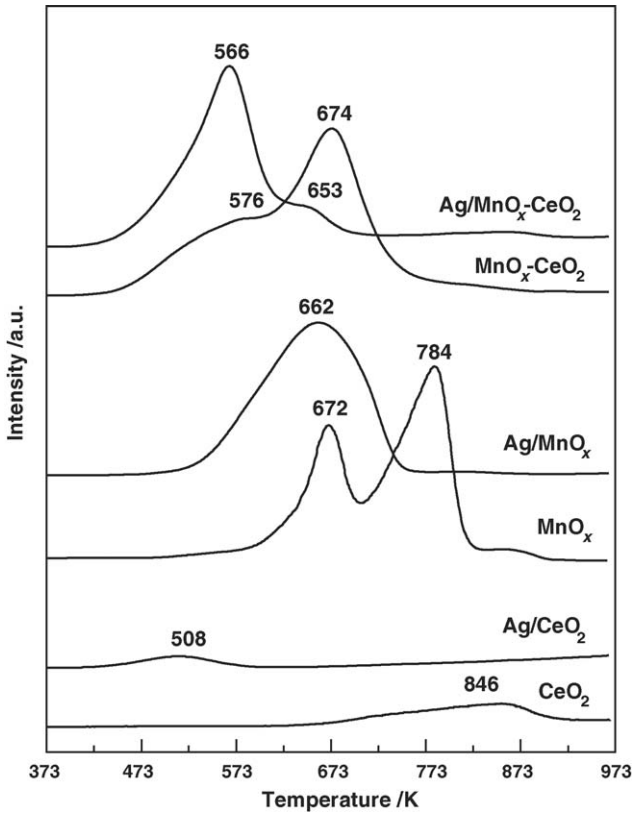

Fig. 2. H_2-TPR profiles of the oxides and the Ag catalysts.

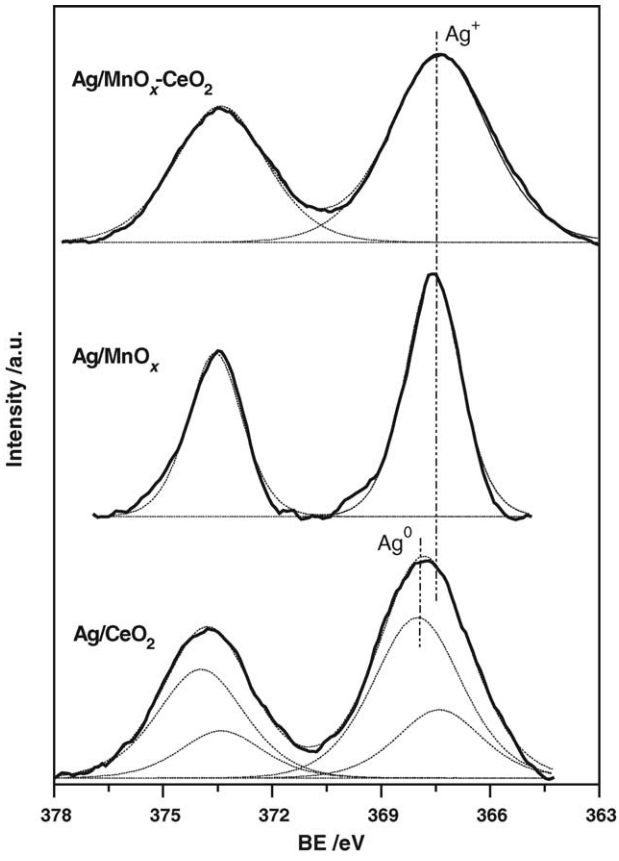

Fig. 3. XPS spectra of Ag 3d of the silver-containing catalysts.

of about 1:2. This is the typical feature of two-step reduction of Mn_2O_3, the low-temperature reduction peak represented the reduction of Mn_2O_3 to Mn_3O_4 and the high-temperature reduction peak referred to the further reduction of Mn_3O_4 to MnO. Previous studies also revealed that the reduction of bulk MnO_2 and/or Mn_2O_3 took place through a distinct two-step process [20–22]. For the MnO_x–CeO_2 mixed oxide, one broad reduction peak starting at 473 K, with a maximum at 576 K, was clearly observed, and followed by another intensive reduction at 674 K. According to the reduction characteristics of pure MnO_x and CeO_2, it can be deduced that the broad peak at 576 K in the TPR profile of MnO_x–CeO_2 corresponded to the reduction of Mn_2O_3 to Mn_3O_4, and the high-temperature reduction peak at 674 K represented the combined reductions of Mn_3O_4 to MnO and the surface Ce^{4+} species. Moreover, the reduction temperatures of the MnO_x–CeO_2 mixed oxide systematically shifted to the lower temperature regions compared with the reduction characteristics of pure Mn_2O_3 and CeO_2. This significant decrease of reduction temperature indicated that the reduction of the manganese oxide and the cerium oxide in the mixture was promoted due to the formation of the solid solution, which facilitated the mobility of the oxygen species in the mixed oxide.

After the addition of silver, the reduction features of the oxides were dramatically modified, depending on the support employed. The H_2-TPR of the Ag/CeO_2 exhibited one broad and relatively weak reduction peak at 508 K, indicating the simultaneous reductions of Ag_2O and surface oxygen of CeO_2. In the case of Ag/MnO_x, only one broad strong reduction peak at 662 K was observed, which could be attributed to the combined reduction of Mn_2O_3 to MnO and dispersed Ag_2O to Ag [23]. The Ag/MnO_x–CeO_2 catalyst showed one intensive reduction peak at about 566 K with a weak shoulder peak at about 653 K. Obviously, the presence of silver greatly shifted the reduction temperatures to lower regions, indicating the occurrence of metal–support interaction between silver and MnO_x–CeO_2. This phenomenon is often interpreted in terms of the activation and spillover of hydrogen from the initially reduced silver to manganese and cerium oxides, and consequently promoted their reductions [14]. However, it is difficult to exactly describe the two reduction peaks due to the formation of MnO_x–CeO_2 solid solution and the hydrogen spillover from silver to the solid solution. Possibly, the main reduction peak at 566 K can be attributed to both the reduction of MnO_x to MnO and dispersed Ag_2O to Ag, while the shoulder reduction peak may be related to the partial reduction of CeO_2.

3.2. Surface properties of the Ag catalysts

Fig. 3 shows the XPS spectra of Ag 3d in the silver-containing catalyst. For the Ag/CeO_2 catalyst, deconvolution of the Ag 3d peaks showed the simultaneous presence of cationic (about 30%) and metallic silver (about 70%). The component centering at 368.0 eV indicated the presence of metallic silver, and the component centering at 367.5 eV could be reasonably attributed to Ag^+, following the previous assignments [24,25]. The Ag $3d_{5/2}$

peak was located at 367.6 eV in the Ag/MnO_x catalyst, demonstrating that only Ag^+ species was present. Similarly, only the Ag $3d_{5/2}$ peak in the Ag/MnO_x–CeO_2 catalyst was detected at 367.5 eV, suggesting the existence of Ag^+ species. It is well known that Ag_2O can be decomposed completely into metallic Ag and O_2 when calcined at temperatures higher than 673 K in air [24,26]. However, the oxidation state of the silver species was still maintained in the Ag/MnO_x–CeO_2 catalyst, which was calcined at 773 K in air. Hence, it can be speculated that the generation of Ag^+ species is arised from the strong interaction between silver and MnO_x–CeO_2 solid solution, through which the active oxygen species on the surface of Mn–Ce mixed oxide is transferred to silver and oxidize it into Ag^+.

Fig. 4 shows the XPS spectra of O 1s in the Ag catalysts. Clearly, two surface oxygen species could be distinguished by deconvoluting the O 1s spectra. The lower binding energy of 528.9–529.5 eV could be ascribed to the lattice oxygen (O^{2-}) [13,27,28] (hereafter denoted as O_α) and the higher binding energy of 531.3–531.8 eV might be assigned to the defect oxides or the surface oxygen ions with low coordination (hereafter denoted as O_β) [13,29,30]. Table 2 lists the typical binding energies of O 1s, Mn $2p_{3/2}$ and Ce $3d_{5/2}$ as well as the relative surface concentration of O_α. The binding energies of Mn $2p_{3/2}$ in the manganese-containing samples all located in 641.5–641.6 eV, which are in good agreement with those reported for Mn_2O_3 [31,32]. The binding energies of Ce^{4+} are located at the characteristic values of 882.4–882.6 eV [30]. The relative concentrations of O_α were calculated to be 42.9, 75.5 and 54.1% for the MnO_x, CeO_2 and MnO_x–CeO_2, respectively. The subsequent addition of silver to the oxides caused these values increase to 45.7, 81.7 and 86.2%. Particularly, the percentage of O_α species in the Ag/MnO_x–CeO_2 catalyst greatly enhanced and approached to 86%. Thus, it seems true that the addition of silver to the oxides caused the generation of more lattice oxygen species through the interactions between silver and the oxides, especially in the Ag/MnO_x–CeO_2 system.

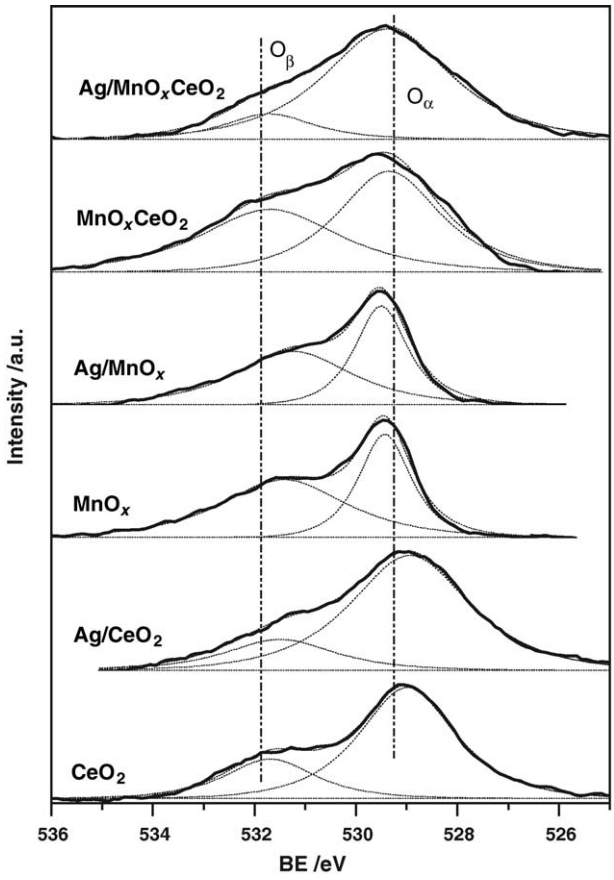

Fig. 4. XPS spectra of O 1s of the Ag catalysts.

3.3. Catalytic activity

Fig. 5 presents formaldehyde conversions over the catalysts as a function of reaction temperature. Clearly, pure CeO_2 and MnO_x gave very low HCHO conversions and the complete oxidations of formaldehyde into H_2O and CO_2 were not achieved even at 493 K. Complete conversion of HCHO was obtained at about 423 K over the MnO_x–CeO_2 mixed oxide, indicating the pronounced catalytic activity of this mixed oxide mainly through the formation of the solid solution between CeO_2 and MnO_x. Noticeably, the addition of silver significantly improved the catalytic activities of the oxides. The complete oxidations of HCHO over the Ag/CeO_2 and Ag/MnO_x catalysts were achieved around 393 and 413 K, respectively. Most promisingly, the complete oxidation of HCHO over the Ag/MnO_x–CeO_2 catalyst was achieved at temperature as low as 373 K, implying that a synergetic effect among silver, manganese and cerium oxides may exist in the Ag/MnO_x–CeO_2 system. As a matter of fact, this interaction can be interpreted in terms of an oxygen transfer mechanism relating to the oxygen mobility through the

Table 2
XPS results of the samples

Sample	BE (eV)		$O_\alpha/(O_\alpha+O_\beta)$[a] (%)	Mn $2p_{3/2}$ (eV)	Ce $3d_{5/2}$ (eV)
	O_α	O_β			
MnO_x	529.5	531.3	42.9	641.5	–
Ag/MnO_x	529.5	531.4	45.7	641.5	–
CeO_2	528.9	531.6	75.5	–	882.6
Ag/CeO_2	529.0	531.5	81.7	–	882.4
MnO_x–CeO_2	529.3	531.8	54.1	641.6	882.6
Ag/MnO_x–CeO_2	529.4	531.7	86.2	641.6	882.6

[a] O_α represents the lattice oxygen species and O_β refers to other oxygen species.

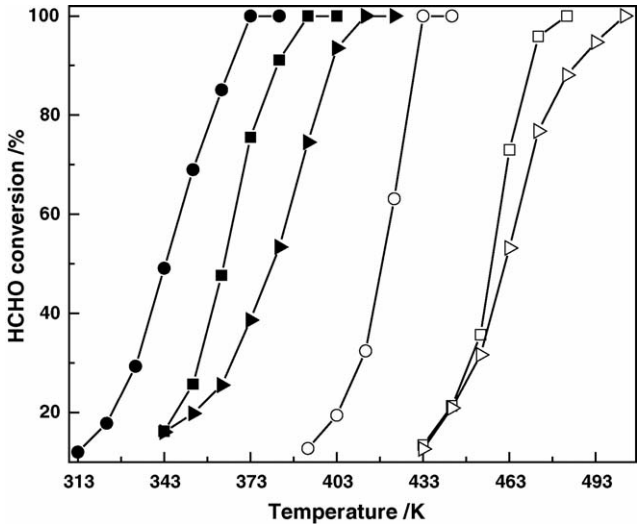

Fig. 5. Temperature dependence of HCHO conversions over the Ag catalysts: Ag/MnO_x–CeO_2 (●); Ag/CeO_2 (■); Ag/MnO_x (►); MnO_x–CeO_2 (◯); MnO_x (□); CeO_2 (△). Reaction conditions: HCHO = 580 ppm, O_2 = 18.0%, He balance, GHSV = 30,000 mL/(g_{cat} h).

redox cycles of Ag^+/Ag^0, Mn^{4+}/Mn^{3+} and Ce^{4+}/Ce^{3+}, as shown below.

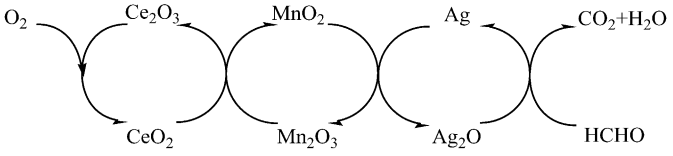

Initially, the oxygen species released from the decomposition of Ag_2O participated in the oxidation of formaldehyde [33,34], and the reoxidation of Ag to Ag_2O would be achieved via the oxygen species from MnO_2. Simultaneously, the regeneration of the produced Mn_2O_3 to MnO_2 would be realized via the oxygen species from the oxygen reservoir of CeO_2, and the Ce_2O_3 thus formed can be reoxidized into CeO_2 by the oxygen in the feed stream. This proposed oxygen transfer mechanism can be evidenced by previous observations. Imamura has found that cerium oxide, based on its well-known oxygen storage capacity, could provide oxygen to MnO_x for increasing the valence of manganese in MnO_x–CeO_2 mixed oxide [35]. It was also reported that manganese oxide could supply oxygen to the silver on the surface of an Ag/MnO_x catalyst, so that the oxidation state of silver could be maintained [36]. For the present Ag/MnO_x–CeO_2 catalyst, it is reasonable to say that the activation of the oxygen molecules participating in the HCHO oxidation reaction is a synergetic process by considering the structural characteristics obtained by XPS and TPR measurements. CeO_2, which is the well known to possess oxygen storage capacity, will interact with the oxygen molecules in the reaction stream through the redox cycle of Ce^{4+}/Ce^{3+} and provide oxygen species to the Mn_2O_3, resulting in the realization of recycling of Mn_2O_3 to MnO_2. Meanwhile, the MnO_2 will supply oxygen to the silver nearby, thus maintains the recycling of the oxidation state of silver, which is responsible for the oxidation of formaldehyde. Hence, transfer of oxygen from the oxygen reservoir CeO_2 to the active sites of Ag_2O through the MnO_x can effectively facilitate the activation of molecular oxygen.

The oxygen activation and its transfer between the support and the active metal should be strongly dependent on the redox properties of the catalyst. As a matter of fact, the extremely high catalytic activity of the Ag/MnO_x–CeO_2 catalyst is in good accordance with its reduction at much lower temperatures, as shown in the TPR profiles. That is, the reduction behavior is intimately related to the catalytic performance of the Ag/MnO_x–CeO_2 catalyst. Probably, the easy reduction of the Ag/MnO_x–CeO_2 catalyst leads to the easier activation and transformation of the oxygen species between the MnO_x–CeO_2 solid solution and the surface silver species, and consequently results in the higher catalytic activity for the HCHO oxidation. Additionally, the high catalytic activity of the Ag/MnO_x–CeO_2 is also in consistent with the relatively high concentration of the O_α lattice oxygen species, as demonstrated by the XPS measurements. The oxygen species over silver have been previously classified into two main categories: the "ionic" or nucleophilic oxygen species with BE of 528.4–530.0 eV (O_α) and the "covalent" or electrophilic oxygen species with BE of 530.5–532.0 eV (O_β), and the former is responsible for complete oxidation, while the latter plays a key role in partial oxidation reactions [37–40]. Furthermore, the carbonyl group of formaldehyde provides an electrophilic site to allow it to react easily with the nucleophilic O_α species on the surface of the catalysts. Therefore, by increasing the abundance of the O_α species, it will greatly favor the oxidation of formaldehyde. This also provides a good interpretation for the high activity of the Ag/MnO_x–CeO_2 catalyst.

4. Conclusion

Complete oxidation of formaldehyde was achieved at temperature as low as 373 K over the Ag/MnO_x–CeO_2 catalyst. Structure analysis by XRD, TPR and XPS measurements revealed that the formation of solid solution in the MnO_x–CeO_2 mixed oxide greatly improved the interaction between MnO_x and CeO_2, and the consequent addition of silver was highly dispersed on the surface of the solid solution. The effective activation of molecular oxygen in the reactants through the oxygen transfer mechanism was crucial for the complete oxidation of formaldehyde. The consecutive transfer of oxygen from the oxygen reservoir CeO_2 to the active center Ag_2O through MnO_x presumably facilitates the complete oxidation of formaldehyde at lower temperatures.

References

[1] R.J. Shaughnessy, E. Levetin, J. Blocker, K.L. Sublette, Indoor Air 4 (1994) 179–188.
[2] H. Nakayama, A. Hayashi, T. Eguchi, N. Nakamura, M. Tsuhako, Solid State Sci. 4 (2002) 1067–1070.
[3] S. Imamura, Y. Uematsu, K. Utani, T. Ito, Ind. Eng. Chem. Res. 30 (1991) 18–21.
[4] K.T. Chuang, B. Zhou, S.M. Tong, Ind. Eng. Chem. Res. 33 (1994) 1680–1686.
[5] M.C. Álvarez-Galván, B. Pawelec, V.A. de la Peña O'Shea, J.L.G. Fierro, P.L. Arias, Appl. Catal. B 51 (2004) 83–91.
[6] C.B. Zhang, H. He, K.-i. Tanaka, Catal. Commun. 6 (2005) 211–214.
[7] S. Imamura, D. Uchihori, K. Utani, Catal. Lett. 24 (1994) 377–384.

[8] Y. Sekine, A. Nishimura, Atmos. Environ. 35 (2001) 2001–2007.
[9] Z.Y. Ding, L.X.D. Wade, E.F. Gloyna, Ind. Eng. Chem. Res. 37 (1998) 1707–1716.
[10] S. Aki, M.A. Abraham, Ind. Eng. Chem. Res. 38 (1999) 358–367.
[11] H. Chen, A. Sayari, A. Adnot, F. Larachi, Appl. Catal. B 32 (2001) 195–204.
[12] A.M.T. Silva, R.R.N. Marques, R.M. Quinta-Ferreira, Appl. Catal. B 47 (2004) 269–279.
[13] X.F. Tang, Y.G. Li, X.M. Huang, Y.D. Xu, H.Q. Zhu, J.G. Wang, W.J. Shen, Appl. Catal. B 62 (2006) 265–273.
[14] S. Hamoudi, A. Sayari, K. Belkacemi, L. Bonneviot, F. Larachi, Catal. Today 62 (2000) 379.
[15] H.P. Klug, L.E. Alexander, X-Ray Diffraction Procedures, John Wiley, New York, 1954.
[16] M. Machida, M. Uto, D. Kurogi, T. Kijima, Chem. Mater. 12 (2000) 3158–3164.
[17] S. Imamura, H. Yamada, K. Utani, Appl. Catal. A 192 (2000) 221–226.
[18] A. Trovarelli, Catal. Rev. Sci. Eng. 38 (1996) 439–520.
[19] E. Aneggi, M. Boaro, C. de Leitenburg, G. Dolcetti, A. Trovarelli, J. Alloys Compd. 408–412 (2006) 1096–1102.
[20] F. Kapteijn, L. Singoredjo, A. Andreini, Appl. Catal. B 3 (1994) 173–189.
[21] J. Carnö, M. Ferrandon, E. Björnbom, S. Järås, Appl. Catal. A 155 (1997) 265–281.
[22] J. Trawczyński, B. Bielak, W. Miśta, Appl. Catal. B 55 (2004) 277–285.
[23] R. Lin, W.P. Liu, Y.J. Zhong, M.F. Luo, Appl. Catal. A 220 (2001) 165–171.
[24] J.F. Weaver, G.B. Hoflund, J. Phys. Chem. 98 (1994) 8519–8524.
[25] J.S. Hammond, S.W. Gaarenstroom, N. Winograd, Anal. Chem. 47 (1975) 2193–2199.
[26] G.I.N. Waterhouse, G.A. Bowmaker, J.B. Metson, Phys. Chem. Chem. Phys. 3 (2001) 3838–3845.
[27] A. Bensalem, F. Bozon-Verduraz, M. Delamar, G. Bugli, Appl. Catal. A 121 (1995) 81–93.
[28] S. Hamoudi, F. Larachi, A. Adnot, A. Sayari, J. Catal. 185 (1999) 333–344.
[29] J.P. Holgado, G. Munuera, J.P. Espinós, A.R. González-Elipe, Appl. Surf. Sci. 158 (2000) 164–171.
[30] F. Larachi, J. Pierre, A. Adnot, A. Bernis, Appl. Surf. Sci. 195 (2002) 236–250.
[31] B.R. Strohmeier, D.M. Hercules, J. Phys. Chem. 88 (1984) 4922–4929.
[32] V. Di Castro, G. Polzonetti, J. Electron. Spectrosc. Relat. Phenom. 48 (1989) 117–123.
[33] A. Andreasen, H. Lynggaard, C. Stegelmann, P. Stoltze, Surf. Sci. 544 (2003) 5–23.
[34] L. Kundakovic, M. Flytzani-Stephanopoulos, Appl. Catal. A 183 (1999) 35–51.
[35] S. Imamura, Ind. Eng. Chem. Res. 38 (1999) 1743–1753.
[36] N. Watanabe, H. Yamashita, H. Miyadera, S. Tominaga, Appl. Catal. B 8 (1996) 405–415.
[37] V.I. Bukhtiyarov, A.F. Carley, L.A. Dollard, M.W. Roberts, Surf. Sci. 381 (1997) L605–L608.
[38] V.I. Bukhtiyarov, V.V. Kaichev, J. Mol. Catal. A 158 (2000) 167–172.
[39] A.I. Boronin, S.V. Koscheev, V.F. Malakov, G.M. Zhidomirov, Catal. Lett. 47 (1997) 111–117.
[40] A.I. Boronin, S.V. Koscheev, G.M. Zhidomirov, J. Electron. Spectrosc. Relat. Phenom. 96 (1998) 43–51.